Array Thinning by Using Antennas in a Fabry–Perot Cavity for Gain Enhancement

Renato Gardelli, Matteo Albani, *Member, IEEE*, and Filippo Capolino, *Senior Member, IEEE*

***Abstract*—A Fabry–Perot cavity (FPC) between a ground plane and a partially reflective surface (PRS) is used here to design array antennas with large distance between the radiating elements. This configuration provides some advantages: i) a reduction of the number of array elements to achieve high directivity; ii) large space between contiguous elements that may host a bulky feeding network as required for dual polarization or active antennas; iii) small coupling and easy feeding network designs because of the smaller number of elements with larger inter-element distance. We show that when designing the FPC antenna a frequency shift of the gain maximum may occur, especially in this sparse array configuration. We also show the existence of preferred distances between elements that controls both the directivity and the side lobe level, and how the presence of the FPC and the relaxed requirement of the interelement distance result in a lower interelement coupling. The presented dual polarized antenna comprises two interleaved 2×2 arrays placed in a 2-layer FPC, and exhibits a 19 dBi gain and 30 dB of isolation between the two ports over an operating bandwidth of approximately 5.7%, i.e., typical for patch antennas.**

***Index Terms*—Antenna arrays, electromagnetic bandgap materials, enhanced directivity, Fabry–Perot cavities (FPC), leaky wave antennas.**

I. Introduction

THE enhancement of directivity by using leaky wave antennas has been a subject of study in the last 40-50 years [1]–[5] and various geometries have been proposed. In the last twenty years attention has been brought also to planar structures made of dielectric layers [6]–[18], [34] called 2-D leaky wave antennas. The enhanced directivity is based on the excitation by a single radiator of a leaky wave along the antenna geometry, that is a complex modal solution allowed to propagate in the structure. In [9]–[18], [34] it has been shown that planar antennas with leaky waves with small propagation constant can produce narrow beams at broadside. Various configurations have been considered to enhance the directivity at broadside, such as single or multi dielectric layers to form a cavity resonator often called Fabry–Perot cavity (FPC). This structure is mainly formed by a half wavelength chamber between a ground plane and a partially reflective surface (PRS) located on top of the cavity. The leaky wave is trapped between the ground plane and the above PRS. In the original studies the top PRS was formed by alternating high-density and low-density quarter wavelength dielectric layers [9]–[12] or with a periodic screen [13]. In the past years the PRS has been often made of planar periodic structures, made of a thin sheet of periodic slots, dipoles or other more complex geometries [13]–[15]. In [16] it has been shown that the phenomenology and design criteria of a PRS made of multiple layer is equivalent to that made of a shunt admittance that is a good model to represent a thin periodic reactive screen such as a frequency selective surface. An in-depth analysis of the fundamental properties of enhanced broadside radiation is carried out in [18], [34] though the main idea was established already at the time of [9].

More recently, the superstrates that constitute the PRS of the FPC, made of multiple layers of homogeneous dielectric material, have been regarded as electromagnetic band gap (EBG) superstrates [19], [20]. Such superstrates have also been realized by more complex EBG materials that are periodic along the longitudinal and transverse (parallel to the antenna plane) directions [21]–[26]. EBG materials have also been used as substrates and radomes [27], [28].

Antennas with enhanced directivity have been proposed in [29], [30] where the homogeneous FPC covered by a PRS is substituted by a metamaterial with low effective permittivity or by an EBG material with a particular dispersion diagram. However the basic principle that produces the enhanced directivity is still based on the excitation of leaky waves as it has been shown in [2], [31], [32].

Although in line of principle the source directivity could be unlimitedly enhanced, a strong directivity results in a very small antenna bandwidth and a very critical design. As shown in this paper, this trade-off between directivity enhancement and bandwidth suggests to use a sparse array inside the FPC that is designed to produce a moderately enhanced directivity for *each* array elements. Such a configuration allows to preserve the needed operating bandwidth and achieve the requested directivity by using sparse arrays of sources. Since each element in the FPC is individually quite directive, a larger spacing between elements is permitted still avoiding grating lobes. The thinning of the array elements results in a simpler structure with fewer elements, a simpler feeding network and a lower coupling between elements as it is shown in this paper. In Sections II–V we investigate the abovementioned issues showing by some examples how the use of an FPC allows to decimate the radiators in a standard spaced array without degrading the pattern characteristics, especially focusing on coupling, side lobes, and gain effects. In Section II we analyze the frequency shift of the gain maximum with respect to the design frequency when using both ideal radiators and patch antennas. This shift should be accounted for when designing sparse arrays. In Section V we

Manuscript received August 15, 2005; revised January 23, 2006. This work was supported by the EU-funded project METAMORPHOSE (FP6/NMP3-CT-2004-500252).

R. Gardelli and M. Albani are with the Dipartimento di Fisica della Materia e Tecnologie Fisiche Avanzate Università di Messina, I-98166 Messina, Italy (e-mail: malbani@ingegneria.unime.it).

F. Capolino is with the Dipartimento Ingegneria dell'Informazione, Università di Siena, I-53100, Siena, Italy (capolino@dii.unisi.it).

Digital Object Identifier 10.1109/TAP.2006.877172

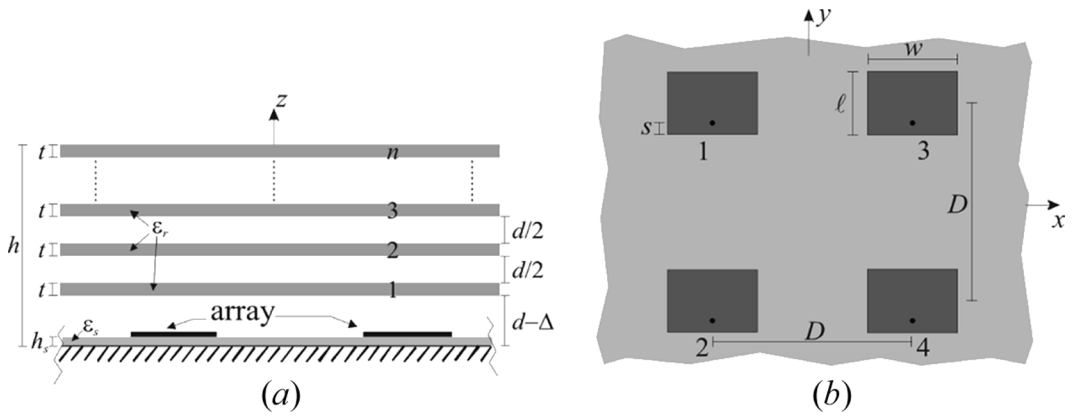

Fig. 1. (a) Lateral and (b) front view of a sparse array in an FPC. The FPC permits larger spacing between elements without the appearance of grating lobes.

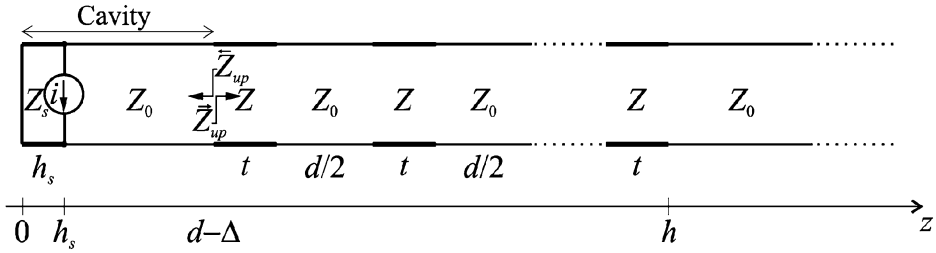

Fig. 2. Modal TL for the calculation of multilayered structure Green's function.

explicitly analyze the performance of the sparse array versus interelement distance for a selected geometry. Furthermore, since a large space is available between elements, an interlaced array can be arranged to achieve dual polarization facilities. In Section VI we present a design example which comprises two interlaced array providing a dual polarized antenna with high decoupling between the two ports.

II. FPC Design: Single Antenna Under an EBG Superstrate

The FPC in Fig. 1 has the advantage of increasing the directivity of a single antenna located inside it [9]–[18], [34]. The antenna excites a leaky mode that produces the broadside pattern, as rigorously demonstrated in [9]–[12], [18], [34]. In those papers the multilayered structure is analyzed with the help of a transmission line (TL) as shown in Fig. 2, which is an effective tool for this kind of structures. Here we use that formalism and we provide some design criteria and numerical examples to show the gain enhancement. As an example, the radiating element is chosen to be a patch antenna printed on a $h_s = 0.762\ \mathrm{mm}(= 30\ \mathrm{mils})$ thick substrate with relative permittivity $\varepsilon_s = 2.5$, fed by a coaxial probe. The multilayered superstrate consists of n layers of dielectric material with relative permittivity ε_r and thickness t, separated by a $d/2$ air gap, with $d = \lambda_0/2$ (Fig. 1). Except where explicitly remarked, in what follows we assume $\varepsilon_r = 2.5$ corresponding to a commercial duroid material. At the operating frequency, which in our examples is fixed to $f_0 = 14\ \mathrm{GHz}$, we have $d = \lambda_0/2 = 10.70\ \mathrm{mm}$, and the choice $t = \lambda/4 = 3.39\ \mathrm{mm}$ and $d/2 = \lambda_0/4 = 5.35\ \mathrm{mm}$ (with $\lambda = 13.54\ \mathrm{mm}$ and $\lambda_0 = 21.41\ \mathrm{mm}$ denoting the wavelength in the dielectric and in free-space, respectively) realizes a $2n-1$ sections quarter-wavelength transformer (for a broadside propagating wave) that reduces the free space radiation resistance by the factor ε_r^n

$$\vec{Z}_{\mathrm{up}} = \frac{Z_0}{\varepsilon_r^n} \tag{1}$$

where $\vec{Z}_{\mathrm{up}}$ is the impedance evaluated at $z = d - \Delta$ looking toward increasing z (Fig. 2). Since we are interested in broadside radiation, all impedances, defined only for plane propagation, are evaluated assuming a plane wave traveling along the direction z, with wavenumber perpendicular to the x, y plane, e.g., $Z_0 = \sqrt{\mu_0/\varepsilon_0}$. From (1), a low impedance $\vec{Z}_{\mathrm{up}}$ is obtained either by a high dielectric permittivity ε_r or by a significant number of layers n. A low value of $\vec{Z}_{\mathrm{up}}$, compared to Z_0, serves to create a PRS at $z = d - \Delta$ to form an FPC in the region $0 < z < d - \Delta$. In [9]–[18], [34] studies have been carried out for cavities without the h_s-thick dielectric layer (used here to support a patch), and the FPC was assumed to have a thickness of $d = \lambda_0/2$. This produces $\overleftarrow{Z}_{\mathrm{up}} = 0$ at $z = d$, that almost matches the low value of $\vec{Z}_{\mathrm{up}}$ in (1). In this paper instead, the presence of the h_s-thick dielectric layer with relative dielectric constant ε_s modifies the height of the FPC and a correction factor Δ must be introduced to maintain the operating frequency equal to f_0. The correction factor depends on the height h_s of the dielectric layer and on its dielectric constant ε_s, and the absence of the dielectric layer (either $h_s = 0$ or $\varepsilon_s = 1$) implies $\Delta = 0$. When the h_s-thick dielectric layer is present (Fig. 1), the condition $\overleftarrow{Z}_{\mathrm{up}} = 0$ is encountered at a distance $z = d - \Delta$, with

$$\Delta = \frac{\lambda_0}{2\pi} \arctan\left[\frac{1}{\sqrt{\varepsilon_s}} \tan\left(\frac{2\pi}{\lambda_0}\sqrt{\varepsilon_s} h_s\right)\right] - h_s. \tag{2}$$

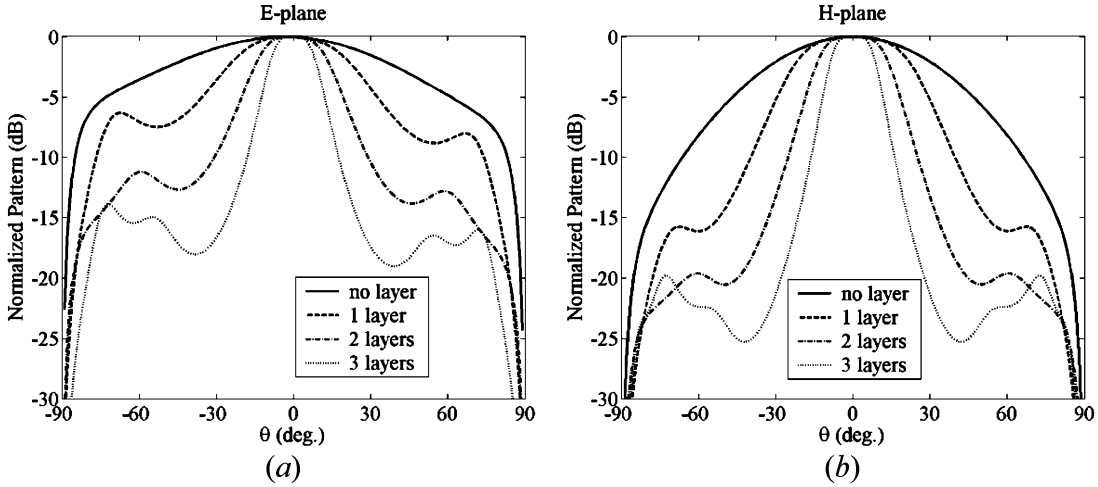

Fig. 3. Far field normalized radiation pattern for a patch in an FPC with various number n of layers, (a) E-plane and (b) H-plane cuts.

TABLE I
FPC PERFORMANCES ($\varepsilon_r = 2.5$)

No. of layers	Max gain	Gain enhancement	Max gain *f*	frequency shift	Gain 3dB bandwidth
1	10.4dB	+3.5dB	13.70 GHz	-300 MHz = -2.2%	3.83 GHz = 28.0%
2	14.1dB	+7.2dB	13.94 GHz	-60 MHz = -0.4%	1.00 GHz = 7.2%
3	17.7dB	+10.8dB	13.97 GHz	-30 MHz = -0.2%	0.35 GHz = 2.5%

The details of its derivation are reported in Appendix A. For small substrate heights h_s, the correction factor in (2) can be approximated as

$$\Delta \approx \frac{h_s^3}{3}\left(\frac{2\pi}{\lambda_0}\right)^2(\varepsilon_s - 1). \tag{3}$$

In our particular case $h_s = 0.762\,\text{mm}$, $\varepsilon_s = 2.5$ and $\lambda_0 = 21.4\,\text{mm}$ ($f_0 = 14\,\text{GHz}$), the correction term becomes $\Delta = 0.78\,\text{mm}$, therefore the air gap between the patch substrate and the first layer at $z = d - \Delta$ has a thickness $d - \Delta - h_s = 9.93\,\text{mm}$. Note that the size of the FPC is determined here by $d - \Delta$, and not by the specific arrangement of the above PRS. In the case of inductive or capacitive PRS the height of the FPC depends on its reactance [16], [17].

The radiating rectangular conducting patch has dimensions $\ell = 6.2\,\text{mm} \times w = 10\,\text{mm}$. The probe is located at $s = 1.3\,\text{mm}$ from the edge of the patch, to match the 50 Ω impedance of the coaxial line. Such feeding point location was designed in the case with $n = 0$ (no layer), but it provides an acceptable matching in all the considered cases $n = 1, 2, 3$ examined next.

In Fig. 3(a) and (b) the far field normalized radiation patterns in the E- and H-planes at the operating frequency $f_0 = 14\,\text{GHz}$ are shown for an increasing number of superstrate layers. The maximum remains at broadside ($\theta = 0$) and the main lobe narrower by increasing the number of layers, showing the increase of directivity.

In Fig. 4, the accepted gain in the boresight direction ($\theta = 0$)

$$G_{\text{acc}} = \frac{S(\theta = 0)4\pi r^2}{P_{\text{acc}}} = \frac{\text{EIRP}(\theta = 0)}{P_{\text{acc}}} \tag{4}$$

is plotted versus frequency for various number n of layers. In (4), $S(\theta = 0) = |E(r, \theta = 0)|^2/(2\eta_0)$ denotes the power density radiated by the antenna at boresight, at a far field distance r, EIRP is the effective isotropic radiated power (see Appendix B for the calculation of the power density at broadside ($\theta = 0$) for the case of an elementary magnetic and electric dipole), and $P_{\text{acc}} = (1 - |\Gamma|^2)P_{\text{in}}$ is the power delivered to (accepted by) the patch via the probe, with P_{in} denoting the power of the incident travelling wave in the coaxial line and Γ the antenna input reflection coefficient. We look at the accepted gain because it is not affected by the antenna impedance mismatch, and it is thus mostly related to the properties of the FPC. Fig. 4 also shows how the bandwidth decreases when increasing the number of layers because the PRS at $z = d - \Delta$ becomes more reflective and the quality factor Q of the FPC increases. Therefore high directivity can only be achieved by reducing the bandwidth as already indicated in [16]–[18], [34] for an ideal dipole excitation. The accepted gain 3 dB-bandwidth is shown in Table I for

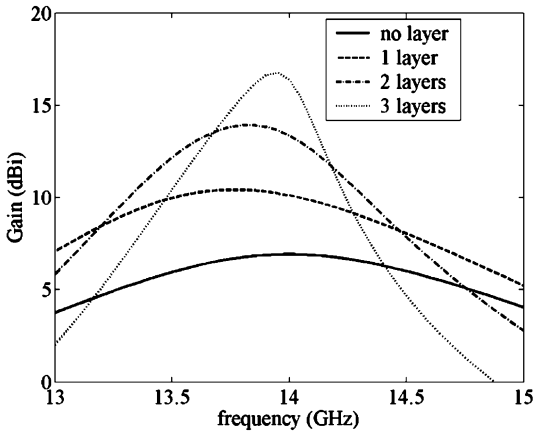

Fig. 4. Broadside accepted gain versus frequency, for a patch inside an FPC with various number n of layers.

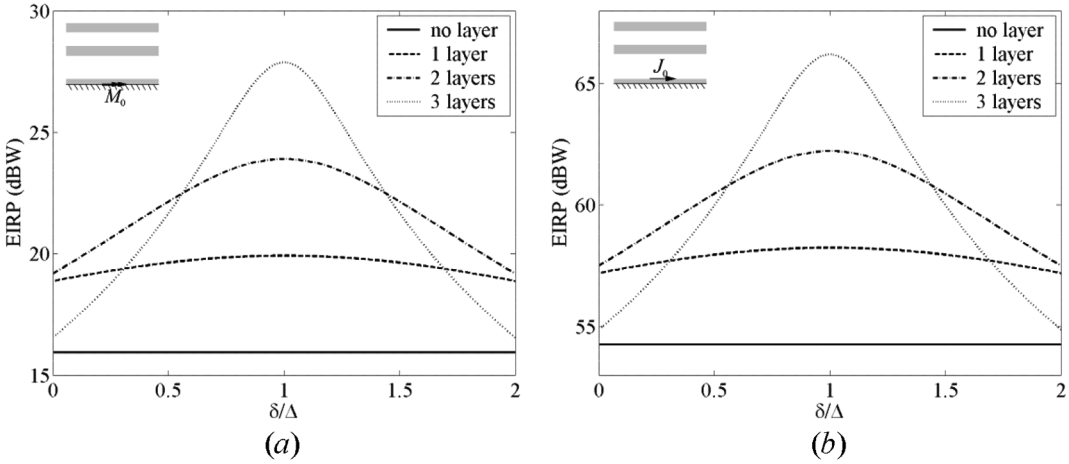

Fig. 5. Broadside EIRP at design frequency f_0 versus cavity size correction δ/Δ, for a unit strength elementary magnetic dipole on the ground plane at (a) $z' = 0$ and for a unit strength elementary electric dipole at patch level (b) $z' = h_s$ inside an FPC with various number n of layers. Δ denote the cavity height correction defined in (2) on the basis of the resonance condition.

various number of layers. Note that the frequency that produces maximum gain is downshifted with respect to the design frequency $f_0 = 14$ GHz, but it approaches f_0 when increasing the number of layers. This is confirmed by the fact that the resonance condition $\overleftarrow{Z}_{\rm up} + \vec{Z}_{\rm up} = 0$ is satisfied exactly only when $\vec{Z}_{\rm up} = 0$ (we recall that we have imposed $\overleftarrow{Z}_{\rm up} = 0$ at f_0), that is achieved only by a total reflective ground plane at $z = d - \Delta$. Indeed, from (1) $\vec{Z}_{\rm up}$ vanishes when either increasing the number of layers n or the dielectric constant of the above n layers. The reason for the downshift of the *gain* is analyzed in the following by resorting to ideal dipole excitations.

It is worth noting that highly resonating (3 layers) FPCs provide large enhancement of the directivity and boresight power density by trapping a lot of reactive energy inside the high Q cavity. Beside a small bandwidth, this may significantly affect the driving element (patch) input impedance that may become difficult to match, thus reducing its impedance bandwidth.

Alternatively, once the operating frequency f_0 has been chosen, the size of the FPC can be determined by maximizing the far field power density at broadside $S(\theta = 0)$ at a given distance r, or equivalently the EIRP, generated by an ideal dipole inside the FPC, following the criterion already been adopted in [9]–[12], [18], [34]. The equivalence of this method with the formula (2) is discussed in the following through numerical calculations. Fig. 5 shows the broadside EIRP at the design frequency f_0 when varying the cavity height, produced by a unit strength elementary magnetic dipole $M_0 = 1\ \mathrm{V}\cdot\mathrm{m}$ at $z' = 0$ [on the ground plane under the substrate, Fig. 5(a)] and by a unit strength elementary electric dipole $J_0 = 1\ \mathrm{A}\cdot\mathrm{m}$ at $z' = h_s$ [on top of the substrate, Fig. 5(b)], in the FPC with various layers, by using the formulas in Appendix B. The results for these kind of sources are expected to be analogous to those for a patch antenna. The numerical investigation to maximize the EIRP is performed by assuming a cavity height $d - \delta$, with δ ranging from 0 to 2Δ where Δ is defined in (2). It is clearly seen that for all the considered number of layers $n = 1, 2, 3$, and for both the kind of sources the maximum EIRP is achieved for $\delta/\Delta = 1$ and thus our resonance condition (2) is equivalent to ensuring a maximum broadside EIRP. Note that the no-layer ($n = 0$) curve in Fig. 5(a) and (b) is also presented as a reference value for the EIRP radiated by the source without the FPC. Then, the EIRP radiated by the two kind of sources at broadside is plotted in Fig. 6 for varying frequency when the cavity is sized according to the optimum value Δ calculated for the design frequency f_0.

As before, Fig. 6(a) and (b) refer to magnetic and electric dipole excitation, respectively. Since the EIRP of a unit strength source depends on the frequency f, the EIRP for a number n of layers is normalized with respect to that for $n = 0$, i.e., without FPC; thus, the no-layer case becomes a 0 dB reference curve for EIRP enhancement due to the FPC. Note that the EIRP enhancement is very similar for the two kind of sources, (a) and (b), and its maximum is in practice at the design frequency f_0. Despite the broadside radiation enhancement is well centered at f_0, the accepted power $P_{\rm acc}$ radiated by the source is varying significantly with frequency, and this causes the sensible *frequency shift* of the gain maximum [see (4)] as shown in Fig. 7 for elementary dipole sources and in Fig. 4 for the patch antenna. Both Fig. 4 and Fig. 7 show the same frequency shift of the *gain* maximum indicating that such an effect is mainly a property of the FPC arrangement, regardless the type of radiating element inside. In Fig. 6(b), the EIRP calculated with the formula (10) in Appendix B is compared with the results from the method of moments (MoM) commercial software Ansoft Designer (marks) to both validate the analysis in Appendix B and check the accuracy of Designer for these particular *resonant* cavities. The agreement is excellent in the scale of the plot.

Estimate of the Antenna Size

In all the above simulations the FPC antenna has an infinite transverse extent as well as in those in the next Sections. In practical implementations the whole structure (size of the dielectric layers and ground plane) shall be truncated at a radial distance L from the source where the field is negligible compared to that at the center of the antenna. Since the magnitude of the field $E(\rho)$ on the aperture is mainly produced by two fundamental TE and TM leaky waves with almost equal attenuation constant α

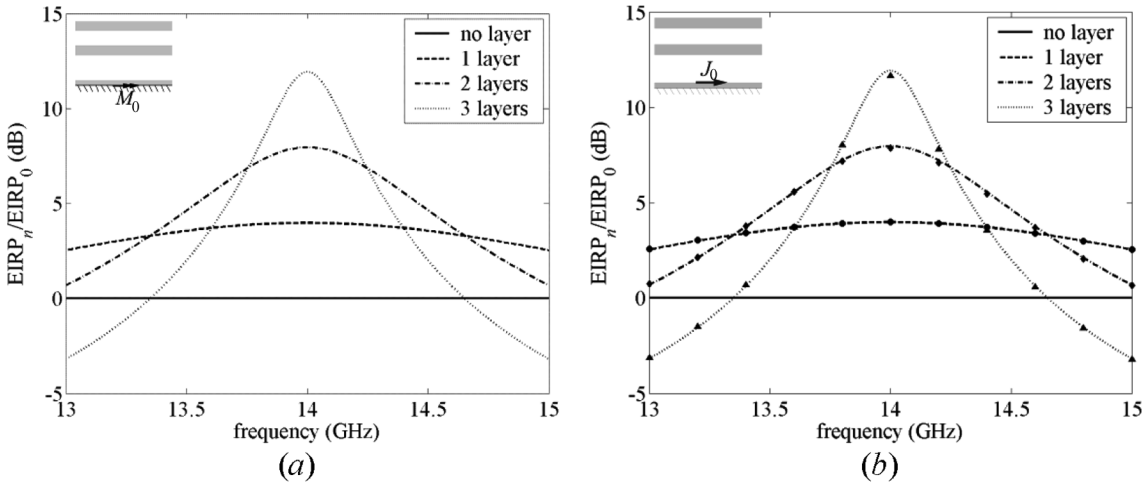

Fig. 6. Normalized broadside EIRP versus frequency, for an elementary magnetic dipole on the ground plane, at (a) $z' = 0$ and for an elementary electric dipole at patch level(b) $z' = h_s$ inside an FPC with various number n of layers. EIRP is normalized with respect to the $n = 0$ (no layer) case. In (b), the results from Ansoft designer are in agreement with (10).

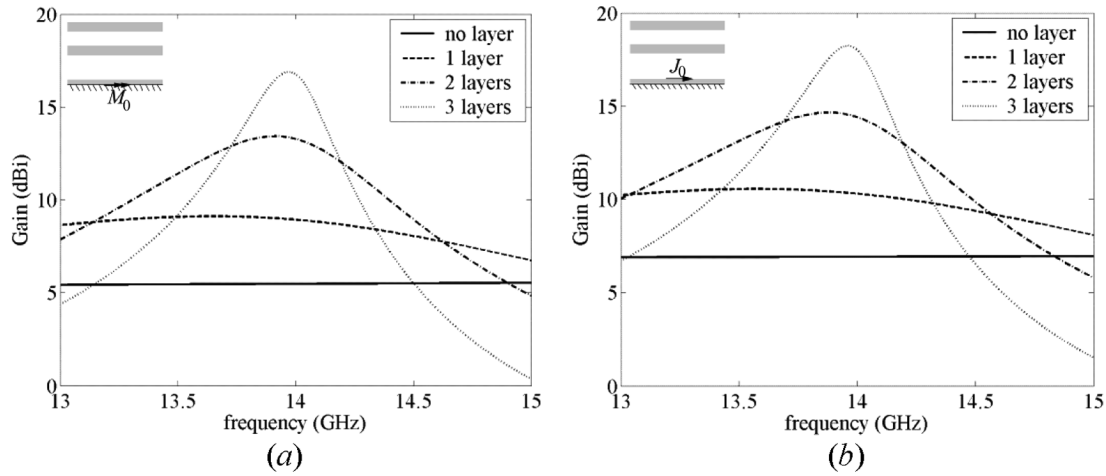

Fig. 7. Broadside accepted gain versus frequency, for an elementary magnetic dipole on the ground plane, at (a) $z' = 0$ and for an elementary electric dipole at patch level (b) $z' = h_s$ inside an FPC with various number n of layers.

[9]–[12] (the approximation $\alpha^{TE} \approx \alpha^{\mathrm{TM}}$ is valid for highly directive antennas), it decays along the radial transverse direction as $E(\rho) \approx E_0 \exp(-\alpha\rho)$, where ρ is the radial distance from the source, and E_0 is the leaky wave value at $\rho = 0$ (other wave species may be important near the source). The value α depends on the antenna design (number of layers and dielectric constants and the antenna size $2L$ is determined by requiring that the field is attenuated by a factor $E(L)/E_0 = \exp(-\alpha L)$ at its edges. Therefore, if one desires the field at the edges of the antenna to be $-X$ dB with respect to its center, the dimension L should be estimated as $L = X/(\alpha 20\log_{10} e) \approx X/(8.686\alpha)$. For instance, for a desired -30 dB edge illumination, $L \approx 3.45/\alpha$. In the case of absence of the patch dielectric layer (in other words, when $\Delta = 0$), the attenuation constant α can be estimated by using the formula [11, Eq. (40)] that in our case is simplified to $\alpha \simeq k_0 \varepsilon_r^{-n/2}\sqrt{2/(\eta_0 F)}$, with $\eta_0 F = \pi[\sqrt{\varepsilon_r}(2\varepsilon_r - 1) + 1]/[(\varepsilon_r - 1)\sqrt{\varepsilon_r}]$ and k_0 the free space wavenumber. Supposing an FPC design with two cover layers $(n = 2)$ with dielectric constant $\varepsilon_r = 2.5$, the formula [11, Eq. (40)] predicts $\alpha \simeq 0.18k_0 = 53.3\ \mathrm{m}^{-1}$ at 14 GHz, and thus 30 dB field reduction is achieved at $L \approx 65$ mm from the center, where the structure can be truncated without affecting the field. A more rigorous numerical analysis where the attenuation constant is determined numerically by imposing $\overleftarrow{Z}_{\mathrm{up}} + \vec{Z}_{\mathrm{up}} = 0$ (taking into account of the thin patch substrate with $h_s = 0.762$ mm and $\varepsilon_s = 2.5$) leads to $\alpha = 0.21k_0 = 61.57\ \mathrm{m}^{-1}$, and thus to a distance $L \approx 56$ mm.

III. Analysis Varying the Dielectric Constant of the Layers

As stated above, the increase of the gain is due to the increase of the reflectivity of the FPC superstrate at $z = d - \Delta$. This is achieved by reducing the equivalent wave impedance $\vec{Z}_{\mathrm{up}}$ in (1) at $z = d - \Delta$ by increasing either the dielectric constant ε_r of the superstrate layers or the number n of layers. In Fig. 8 we show the accepted gain versus frequency for an FPC structure with either (a) two or (b) three layers, for various dielectric constants ε_r available among "Arlon AD" substrates. The dimensions in terms of wavelengths are the same as those in Fig. 1(a); namely, the thickness of the $n = 2$, 3 dielectric layers is $t = \lambda/4$,

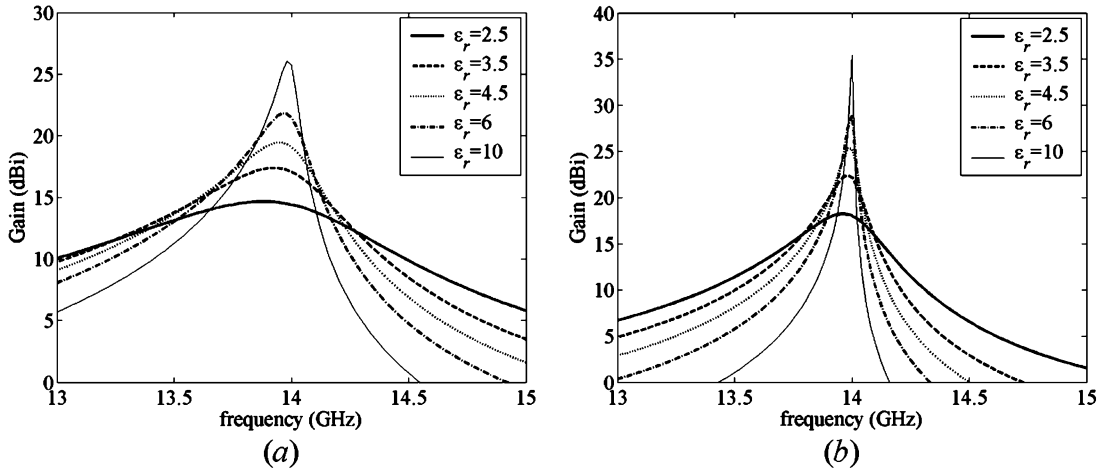

Fig. 8. Broadside accepted gain versus frequency for a patch inside an FPC with (a) $n = 2$ and (b) $n = 3$ layers of different dielectric constant.

with $\lambda = \lambda_0/\sqrt{\varepsilon_r}$ at the operating frequency $f_0 = 14$ GHz, and it thus depends on the material. When the reflectivity of the FPC superstrate at $z = d - \Delta$ is increased by choosing larger ε_r, also the quality factor Q of the FPC is increased, thus resulting in a reduced bandwidth. Note that again the maximum gain (when the size of the cavity is fixed) occurs at frequencies slightly lower than $f_0 = 14$ GHz, but it approaches f_0 when increasing the dielectric constant of the layers. As said above this can be explained by noticing that $\vec{Z}_{\rm up}$ decreases when ε_r increases, therefore better approximating the resonant condition $\overleftarrow{Z}_{\rm up} + \vec{Z}_{\rm up} = 0$.

IV. Array of Antennas Under an EBG Superstrate

Since the above described gain enhancement is obtained to the detriment of the bandwidth, it is not possible to achieve high directivity and large bandwidth at the same time with this type of antennas [16]–[18], [34]. Therefore it may be convenient to use a limited number of layers (say two) to keep a reasonably large bandwidth and to increase the directivity by having an array of a few radiating elements. Such a *sparse* array configuration, with element radiating in the FPC with $n = 2$ and $\varepsilon_r = 2.5$ is compared in the following with a standard *dense* array configuration with no superstrate. Namely, a $D = 0.8\lambda_0 \approx 17$ mm spacing is used for the standard *dense* array with no FPC and a double spacing $D = 1.6\lambda_0 \approx 34$ mm is assumed for the *sparse* array in the FPC. As sketched in Fig. 9 an equivalence in term of radiation properties can be established between a single patch in the FPC and a standard 2×2 array of patches (i.e., with no FPC), as confirmed in Fig. 10 where the accepted gain is plotted versus frequency for both structures. A similar gain level implies a similar effective radiating area. One can see that in Fig. 10, the 2×2 array (with no FPC) has approximately the same gain of the single patch (1×1) inside the FPC. Analogously, the 4×4 array (with no FPC) has approximately the same gain of the 2×2 array inside the FPC. Note that, as expected, the gain-bandwidth of the array with no FPC is larger.

Fig. 11(a) shows that at $f_0 = 14$ GHz the radiation patterns of the 2×2 array (with no FPC) is similar to the one produced by the single patch in the FPC. The main beam is almost coincident in both the E and the H planes. The same radiation pattern equivalence is established in Fig. 11(b), between the 4×4 array (with no FPC) and the 2×2 array in the FPC. Hence the use of the FPC that enhances the gain is adopted to decimate

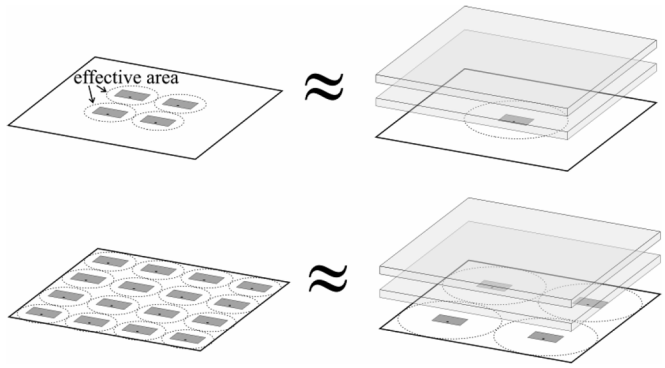

Fig. 9. Sketch of the equivalence between a 2×2 array (with no FPC) and a single patch in an FPC (above), and between a 4×4 array and a 2×2 *sparse* array of patches in an FPC (below).

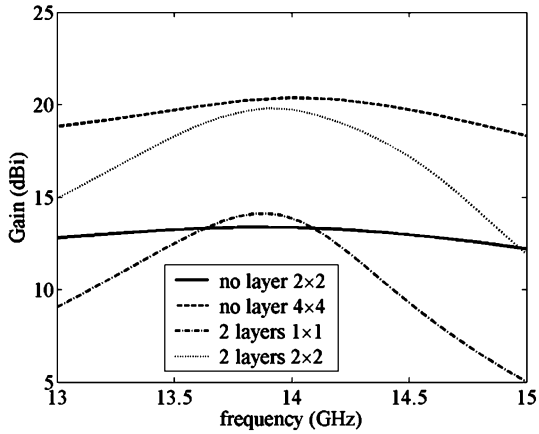

Fig. 10. Broadside accepted Gain versus frequency. 2×2 array (continuous) and 4×4 array (dashed) of patches with no superstrate, single patch, i.e., 1×1, (dash dotted) and 2×2 array (dotted) of patches inside an FPC with $n = 2$ layers.

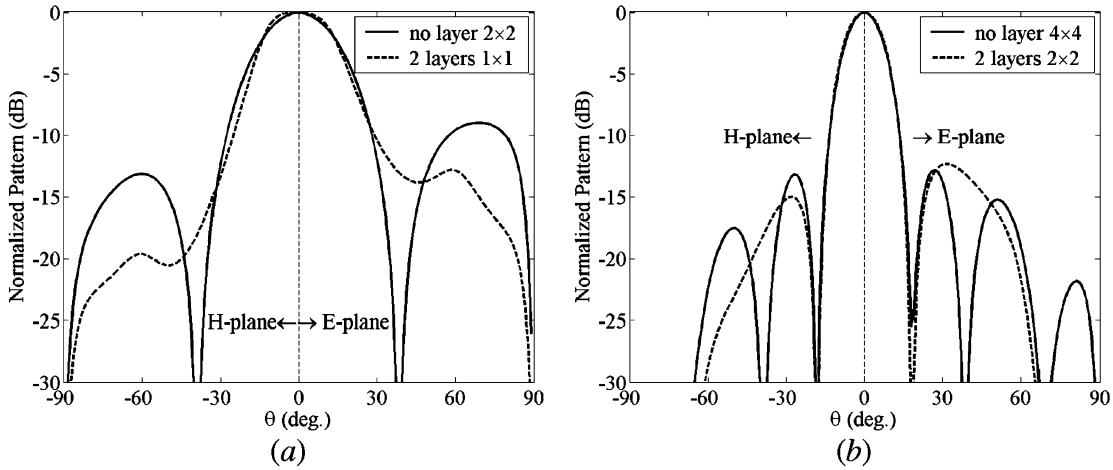

Fig. 11. E- and H- plane normalized radiation patterns for a 2 × 2 (a) and 4 × 4 (b) array of patches without superstrate (continuous line) and for a single patch, i.e., (a) 1 × 1, and (b) 2 × 2 array of patches radiating inside an FPC with $n = 2$ layers (dashed line).

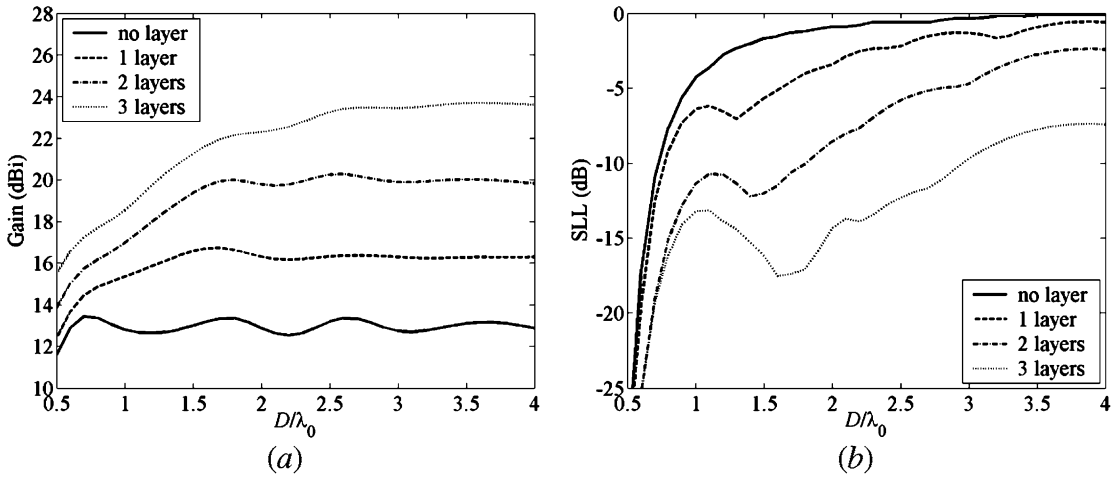

Fig. 12. (a) Accepted gain and (b) SLL versus interelement distance at $f_0 = 14$ GHz, for a 2 × 2 patch array with no superstrate and inside an FPC with $n = 1$, 2, 3 layers.

the radiating elements in an array antenna, thus simplifying their arrangement and the design of their feeding network. In the presented example the decimation ratio is 1:4, however the decimation ratio versus operating bandwidth trade off can be properly fixed by adjusting the FPC gain enhancement effect. Since for resonating antennas, like patches (with no FPC), the frequency range is limited by the impedance bandwidth that is narrower than the pattern bandwidth, a reduction of the pattern bandwidth due to the FPC does not affect the operating bandwidth until the pattern bandwidth becomes smaller than the impedance one. Hence the proposed array thinning does not affect the operating bandwidth up to a certain ratio of thinning.

In what follows, we investigate the radiation properties of the proposed sparse array configuration inside the FPC, by showing how the interelement coupling and radiation features, like gain and sidelobe level, depend on the interelement distance.

V. Analysis of a 2 × 2 Array Characteristics Versus Interelement Distance

We first analyze the radiation gain and side lobe level (SLL) of a 2 × 2 array of patches versus the interelement distance. Such quantities are plotted in Fig. 12 for the various configurations, namely without FPC (no layer) and inside FPCs with $n = 1$, 2 and 3 dielectric layers. As expected, the gain increases by increasing the interelement distance in all the FPC arrangement and tends to reach a limit value corresponding to 6 dB over the single element gain shown in Fig. 4. Indeed, for large-enough interelement distances, the coupling between the elements becomes negligible, so that the power radiated by the array is 4 times the power radiated individually by each element. In the broadside direction, where the element contributions add coherently, the field radiated by the array is 4 times the field radiated by each element and consequently, the broadside power density of the array is 16 times larger than that of each element; hence the array gain is approximately 4 times, i.e., 6 dB more, than that of a single element. The 2 × 2 array radiation pattern presents side lobes corresponding to the array factor grating lobes modulated by the single-element radiation pattern. As a matter of facts, when D/λ_0 approaches unity, the array factor predicts grating lobes at $\theta = \pm 90^\circ$ and the SLL increases for all configurations. Further increasing the interelement distance, the array factor first grating lobes occur at $\theta = \pm\theta_{GL}$ with $\theta_{GL} = \sin^{-1}(\lambda_0/D)$. By choosing D/λ_0 such that θ_{GL} occurs at the element pattern minimum (it is visible in Fig. 3 in both planes, in the range $40^\circ < \theta < 60^\circ$ for the various cases considered), the array factor grating lobes are particularly re-

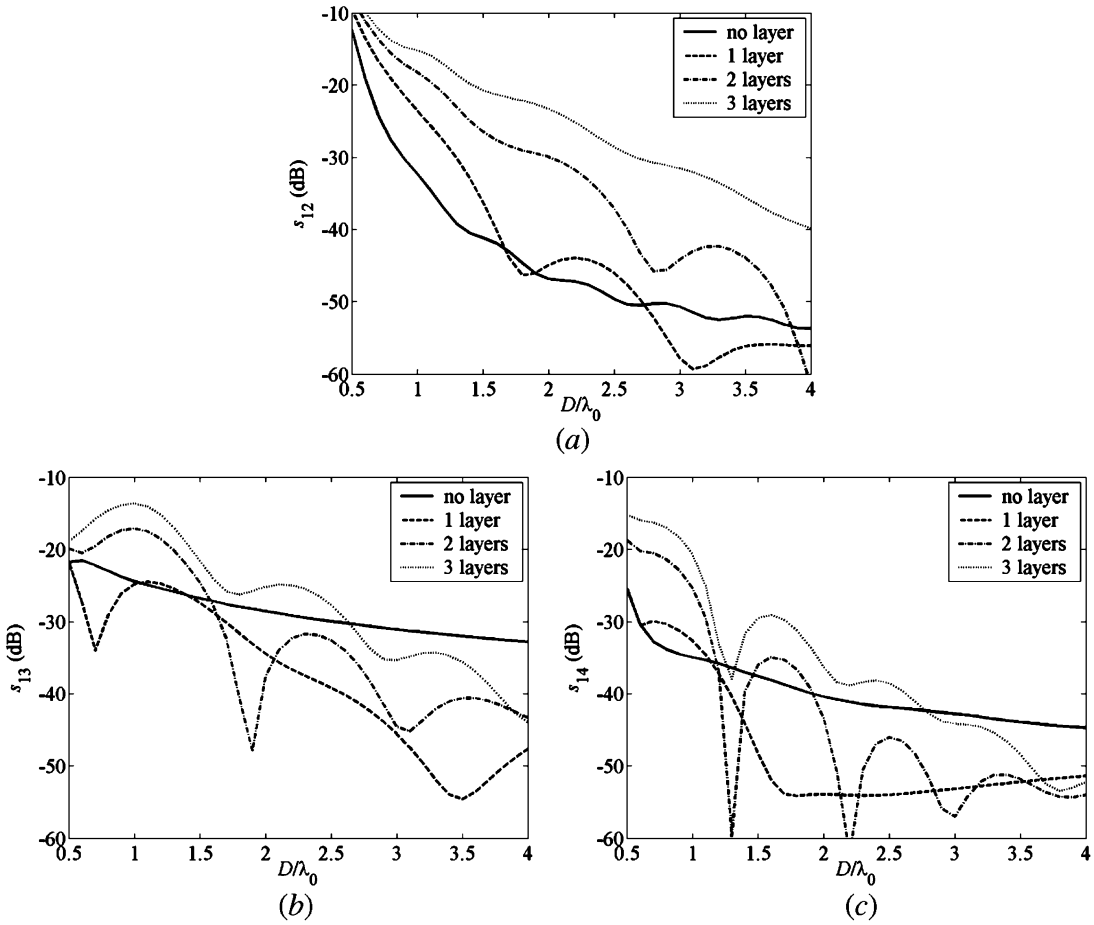

Fig. 13. Coupling scattering parameters (a) s_{12}, (b) s_{13}, and (c) s_{14} versus interelement distance at $f_0 = 14$ GHz, for a 2×2 patch array with no superstrate and inside an FPC with $n = 1, 2, 3$ layers. Element port numbers are indicated in Fig. 1(b).

duced by the element factor hence, in turn, the SLL presents a minimum. Finally, when θ_{GL} enters into the element pattern main lobe (it is shown in Fig. 3), the grating lobes approach the broadside direction and their level grows so that the SLL tends to 0 dB. In summary, the array interelement distance can be chosen in order to maximize the gain, still preserving an acceptable SLL. Focusing now on the 2 layers FPC, it is noticed that for $D = 1.6\lambda_0$ the gain is maximized and the SLL is near the local minimum at $D = \lambda_0/\sin(45°) = 1.4\lambda_0$ (the element pattern in Fig. 3 has a minimum at $\theta \approx 45°$), thus exhibiting a level comparable with that of a standard (without FPC) uniformly illuminated array [cfr. Fig. 11(b)].

Next, in Fig. 13, the coupling scattering parameters between array elements in the different analyzed configurations are plotted versus interelement distance, at the operating frequency $f_0 = 14$ GHz. Element ports are tagged as shown in Fig. 1(b) so that s_{12} and s_{13} are relevant to side by side elements aligned on the H- and E-plane, respectively, whereas s_{14} is relevant to corner by corner elements. When the patches are placed inside the FPC, for a given interelement distance, their coupling increases with the number of layers, i.e., with the reflectivity of the top wall that traps more field around the sources. However, the gain enhancement permits to increase the interelement distance so that the coupling between the elements is dramatically dropped. Furthermore, the interference between *spatial* and *leaky* waves inside the FPC reshapes the s-parameters versus interelement distance behavior creating nulls, i.e., distances for which the element coupling is very weak. In the $n = 2$ layers FPC case, the distance $D = 1.6\lambda_0$ is near to a deep null of the E-plane coupling parameter s_{13}, which is typically the stronger coupling contribution; indeed in standard array configurations, i.e., without the FPC, s_{13} decreases like D^{-1}, whereas on the H-plane the coupling factor s_{12} behaves like D^{-2} due to the null in the space wave radiation pattern. Thereby the array configuration inside an FPC with a $n = 2$ layers and $D = 1.6\lambda_0$ presents a very low interelement coupling (less than -25 dB) and the active reflection coefficient substantially coincides with the isolated element reflection coefficient, thus drastically simplifying the feeding network design.

VI. Dual Polarized Interleaved Sparse Arrays

On the basis of the previous investigations, as an illustrative example, a dual polarized antenna is presented here (see Fig. 14), which consists of two interleaved 2×2 sparse arrays designed and simulated by using the commercial MoM software Ansoft Designer. The multistrate arrangement is still as that in Fig. 1 and comprises the patch substrate with $h_s = 0.762$ mm and $\varepsilon_s = 2.5$ on whose top face patches and feeding lines are printed, and $n = 2$ superstrates with $\varepsilon_r = 2.5$. As explained at the end of Section II, with the help of Fig. 4 and Fig. 7, and

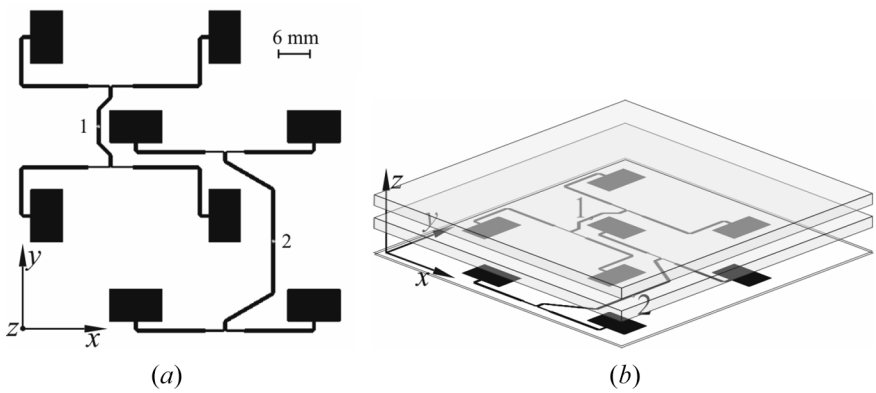

Fig. 14. Dual polarized antenna. Layout (a) 2-D view and complete arrangement (b) 3-D view.

in Appendix B, gain and power enhancement have different frequency dependencies and maximizing the power enhancement at broadside results in a frequency shift of the gain maximum. This is the case of sparse arrays with a significant bandwidth because they are inside FPCs that do not have large Q. In summary, when designing a sparse array a frequency shift may occur when we select the criterion (7). To compensate for the maximum gain frequency shift, the height $d - \Delta$ of the FPC, the thicknesses t of the dielectric superstrates and $d/2$ of the air gap between them are adjusted by increasing the design frequency to 14.1 GHz. Under this condition we obtain $d - \Delta - h_s = 9.85$ mm, $d/2 = 5.32$ mm and $t = 3.36$ mm, and the maximum gain results at the actual operating frequency $f_0 = 14$ GHz. All the patches have dimensions $\ell = 6.05$ mm $\times$ $w = 10$ mm; the small variation in the resonant side length (from 6 mm to 6.05 mm) permits to tune the patch resonance at f_0 when the feed is a coplanar microstrip line instead of the coaxial probe used previously. Both the arrays have a square arrangement with interelement distance $D = 1.6\lambda_0$ and are interlaced in the sense that one patch of an array lies at the center of the other array. The entire printed metallic layout is contained within a $62 \times 62\,\mathrm{mm}^2$ square, and substrates and ground plane are considered infinite with the used MoM software. In practical realizations, truncations effects could be minimized by following the reasoning at the end of Section II; namely the substrates and the ground plane can be truncated at a distance larger than $L = 56$ mm from the patches, to ensure a negligible edge truncation effect. This criterion leads to a overall antenna size of 174×174 mm^2. The patches of the two arrays are oriented orthogonally providing two orthogonally polarized arrays. Each array is fed by a corporate beam forming network printed on the same plane of patches. The microstrip width is $w_m = 0.6$ mm, corresponding to a characteristic impedance of $Z_c = 100\ \Omega$ that matches the input impedance of the patches. Note that due to the low coupling, the patches active input impedance practically coincides with their single element input impedance. Quarter wavelength transformers ($w_m = 0.25$ mm, $Z_c = 140\,\Omega$) realize 3 dB power splits; the junction of two $Z_c = 100\ \Omega$ lines leads to a $Z_{\mathrm{in}} = 50\,\Omega$ input impedance at each probe feed. The antenna matching is provided over a quite wide band $B_{\mathrm{Match}} = 800$ MHz $= 5.7\%$ as shown in Fig. 15 where the scattering parameters at the two probe ports are shown for varying frequency. Note the very low

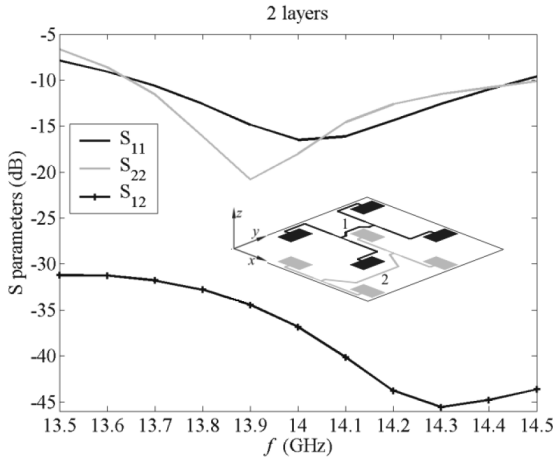

Fig. 15. Scattering parameters at the two ports of the dual polarized antenna.

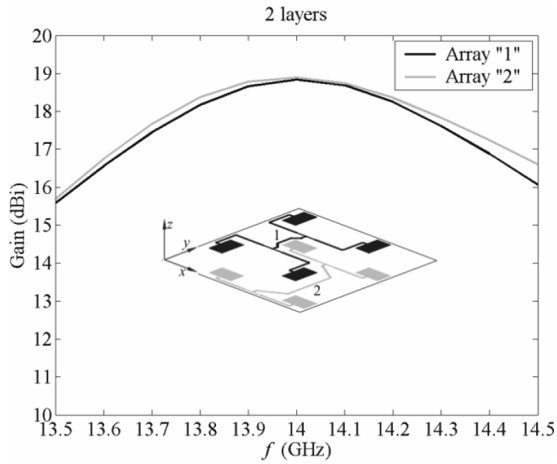

Fig. 16. Gain of the two interleaved arrays forming the dual polarized antenna.

coupling (< -30 dB) obtained between the two 2×2 arrays despite their overlapped arrangement. In Fig. 16, the antenna gain is plotted versus frequency when alternatively feeding port 1 or 2. Note that the actual gain $G_{\mathrm{actual}} = S(\theta = 0)4\pi r^2/P_{\mathrm{in}}$, is plotted here, that also accounts for antenna impedance mismatching because P_{in} is the *incident* power, whilst in the previous figures we have used the accepted gain (4) that has $P_{\mathrm{acc}} =$

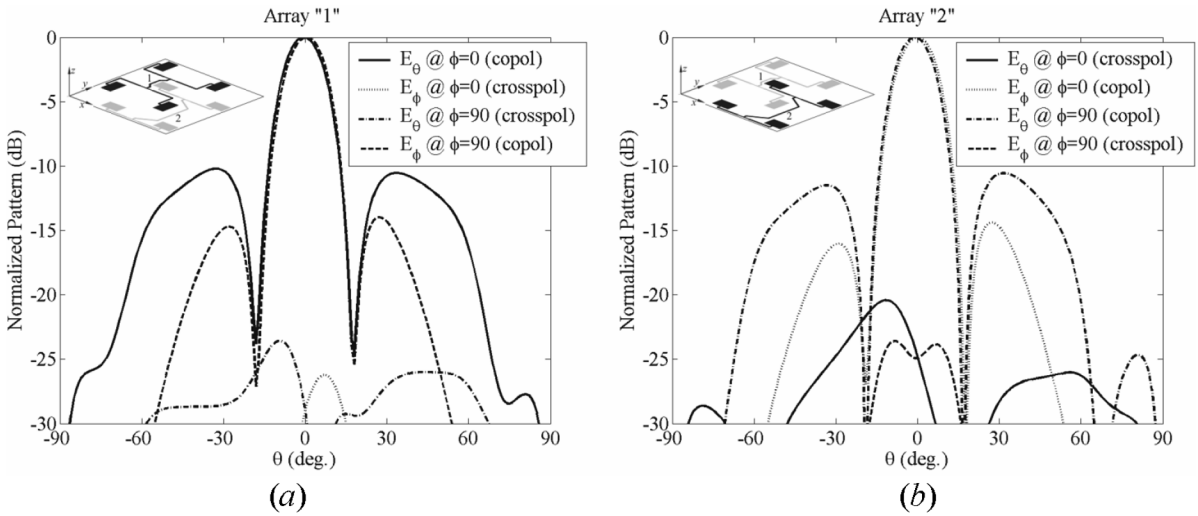

Fig. 17. Normalized radiation patterns of the two arrays forming the dual polarized antenna.

$(1-|\Gamma|^2)P_{\text{in}}$ at the denominator. The two antennas exhibit very similar gain curves with a maximum gain of 19 dB at the center frequency $f_0 = 14\,\text{GHz}$, and the -3 dB gain bandwidth is estimated to be $B_{\text{Gain}} = 800\,\text{MHz} = 5.7\%$. The antenna normalized radiation patterns are plotted in Fig. 17(a) and (b) when transmitting/receiving from port 1 and 2, respectively. The two ports provide analogous radiation patterns with orthogonal polarization, as expected. The co-polar radiation pattern is equivalent to that of a 4×4 array as demonstrated in Fig. 11(b) for individually probe-fed arrays; the cross-polar component is lower than -20 dB, and is mainly due to the feeding network. Higher polarization purity may be easily achieved by laying out the feeding network on a further substrate below the ground plane and feeding the patches by coupling slots etched in the ground plane. Such a solution however results in a more complicated structure.

VII. Conclusion

Highly directive antenna systems are obtained using sparse arrays under a partially reflective superstrate made of a few high permittivity layers to form a FPC. The use of a sparse array with a few layers (say two) permits to achieve a reasonable bandwidth of at least 5.7% and a significant gain at the same time. *Sparse* arrays are made of fewer elements than their *dense* counterpart radiating without FPC, permitting simplified beam forming networks and integration of other devices in the space between the elements. However, in the sparse array configuration the array elements radiate inside a cavity (the FPC) and one may be concerned about their mutual coupling. Interestingly, we have experienced low interelement couplings because of the larger than usual distances used in these sparse arrays, thus permitting a simple design procedure. A simple formula to take into account of the additional patch-substrate thickness is shown in (2), whose derivation is based on the imposed resonant condition (7). However, still a small shift of the operating frequency that yields the gain maximum, from the desired frequency, occurs in the design of sparse arrays because the FPC has not a very large quality factor for obtaining a significant bandwidth.

Though the final design in the present study consists of two interleaved 2×2 arrays, other designs with a larger number of elements could be made when higher directivity is desired.

In general, arrays with high directivity, thus requiring several radiating elements in free space, could be designed by using this kind of partially reflective superstrate with only 1/4 of the elements, at the cost of some bandwidth reduction. However, as pointed out in Section V, some gain benefit due to one or two layers is "free," in the sense that usually the input matching bandwidth is narrower than the pattern bandwidth, and therefore we can increase the gain by using an FPC until the pattern bandwidth is reduced to be equal to the input matching bandwidth.

The main results of this paper, i.e., thinning of the array, dual polarized interleaved array application, design criteria, and a solid analysis of the performances for this class of FPCs comprised of dielectric layers, can be extended to similar geometries where the partially reflective surface is made of a frequency selective surface represented by a shunt admittance, as it has been shown in [16] for an ideal single source excitation.

Appendix A
Resonant Condition

Due to the presence in the FPC of a dielectric substrate of permittivity ε_s and thickness h_s, the height of the FPC has to be adjusted to match the resonance at the design frequency. Resorting to the modal TL model in Fig. 2, the resonance condition is fixed setting the first wavenumber eigenvalue (resonance) of the TL close to the longitudinal wavenumber $k_z = k\cos\theta$ at the design frequency. Since we are interested to broadside radiation $\theta = 0$ for which TE and TM impedance definitions in the TL become equal, the same resonance condition applies to both cases. For lossless non-radiating cavities, eigenvalues are real and it is possible to exactly match the wavenumber k at the design frequency. In our case, due to radiation eigenvalues are complex, thus a perfect match is not possible. Therefore, each observable quantity (modal voltage, current or power at a certain section) will present a (possibly) pronounced peak for frequencies near the resonance frequency but not a singularity. Since these different observable quantities (radiated power, gain, TL

voltages and currents) exhibit different frequency dependencies, each one would have its maximum at a sightly different frequency. However, a high quality factor Q of the FPC ensures very small frequency deviation of the maxima of the various observable quantities, and in practice every quantity presents the peak at the same frequency. Conversely, for FPCs with low Q, the frequency shifts of the various maxima could be significant and these definitions of "resonance" (based on the maxima locations) become ambiguous and dependent on the position of source. For these reasons in the following we adopt a more rigorous and standard definitions of resonance.

The presence of n dielectric layers spaced by air gaps realizes a n-fold impedance transformer, and at the design frequency $f = c/\lambda_0$, with c the free space wavenumber, the impedance looking upward, at the cavity upper level $z = d - \Delta$, with $d = \lambda_0/2$, is (Fig. 1)

$$\vec{Z}(d-\Delta) = \left(\frac{Z}{Z_0}\right)^{2n} Z_0 = \frac{Z_0}{\varepsilon_r^n}. \tag{5}$$

It is a resistance that can be made small by increasing either the layers permittivity ε_r or their number n. Looking downward, at $z = d - \Delta$, the impedance is

$$\overleftarrow{Z}\,(d-\Delta) = \frac{jZ_s \tan[k_s h_s] + jZ_0 \tan\left[k_0(d-\Delta-h_s)\right]}{Z_0 - Z_s \tan[k_s h_s]\tan\left[k_0(d-\Delta-h_s)\right]}, \tag{6}$$

where we have taken into account for the presence of the patch substrate. Thus imposing the resonance condition (for real frequencies)

$$\Im m\left\{\overleftarrow{Z}\,(d-\Delta) + \vec{Z}(d-\Delta)\right\} = 0 \tag{7}$$

leads to the determination of the small correction factor of the cavity thickness

$$\Delta = \frac{1}{k_0}\arctan\left\{\frac{1}{\sqrt{\varepsilon_s}}\tan(k_s h_s)\right\} - h_s. \tag{8}$$

that leads to (2). Note that for $\varepsilon_s = 1$, $\Delta = 0$ as expected.

APPENDIX B
TL EXPRESSIONS FOR THE POWER AT BROADSIDE AND GAIN

After simple treatment of the circuit in Fig. 2 with a TL formalism, the power density at broadside $(\theta = 0)$ normalized with respect to the isotropic spreading [see text after (4)] is expressed as

$$\mathrm{EIRP}(\theta = 0) = \frac{k_0^2}{2\pi\eta_0}|M_0|^2|T|^2_{k_t=0} \tag{9}$$

with $\eta_0 = \sqrt{\mu_0/\varepsilon_0}$ the free space impedance and $k_0 = \omega\sqrt{\mu_0\varepsilon_0}$ the free space wavenumber, for the case of an elementary magnetic dipole M_0 at $z' = 0$, or

$$\mathrm{EIRP}(\theta = 0) = \frac{k_0^2}{2\pi\eta_0}|J_0|^2|\overleftrightarrow{Z}\,T|^2_{k_t=0} \tag{10}$$

for an elementary electric dipole J_0 at $z' = h_s$. In (9) and (10)

$$T = \frac{V(h)}{V(z')} = \frac{Z_0}{Z_0 A + B} \tag{11}$$

denotes the voltage transmission coefficient in the modal equivalent TL of Fig. 2, from the source point z' to the top of the stack of dielectric layers at $z = h$, i.e., at the beginning of the final TL where free-space starts. The transmission coefficient T is directly calculated in terms of the ABCD (transmission matrix) parameters relevant to the section $z' < z \leq h$ of the equivalent TL, and it depends on the longitudinal TL propagation constant $k_z = \sqrt{k_0^2 - k_t^2}$, that in turns depends on the transverse wavenumber k_t, which is set to $k_t = 0$ in (9) and (10) for the broadside direction of observation $\theta = 0$. Furthermore, in (10) $\overleftrightarrow{Z}$ is the total impedance (parallel of upper $\vec{Z}$ and lower $\overleftarrow{Z}$ impedances) at the generator section $z' = h_s$.

The gain is derived by the formula (4), where the accepted power P_{acc} produced by the ideal electric and magnetic dipoles is determined by using a TL formalism. The final expressions are

$$P_{\mathrm{acc}} = \frac{|M_0|^2}{8\pi}\int_0^{+\infty} k_t \Re e\left\{\overleftrightarrow{Y}'\,(k_t) + \overleftrightarrow{Y}''\,(k_t)\right\} dk_t \tag{12}$$

when excited by a magnetic dipole, and

$$P_{\mathrm{acc}} = \frac{|J_0|^2}{8\pi}\int_0^{+\infty} k_t \Re e\left\{\overleftrightarrow{Z}'\,(k_t) + \overleftrightarrow{Z}''\,(k_t)\right\} dk_t \tag{13}$$

when excited by an electric dipole. Here, $\overleftrightarrow{Y}$ and $\overleftrightarrow{Z}$ are the total admittance or impedance evaluated at the source location $z' = 0$ or $z' = h_s$, when excited by the magnetic or the electric dipole, respectively. Primed and double primed symbols refer to transverse magnetic (TM) and transverse electric (TE) quantities, respectively. For the used formalism and notation see [33].

ACKNOWLEDGMENT

The authors are grateful to Prof. D. R. Jackson for useful discussions on the phenomenology of leaky waves and bandwidth properties for these kind of antennas.

REFERENCES

[1] L. O. Goldstone and A. A. Oliner, "Leaky wave antennas I: Rectangular waveguides," *IRE Trans. Antennas Propag.*, vol. AP-7, pp. 307–319, Oct. 1959.
[2] T. Tamir and A. A. Oliner, "The influence of complex waves on the radiation field of a slot-excited plasma layer," *IRE Trans. Antennas Propag.*, vol. AP-10, pp. 55–65, Jan. 1962.
[3] ——, "Guided complex waves. Part I and II," *Proc. Inst. Elect. Eng.*, vol. 110, pp. 310–334, Feb. 1963.
[4] T. Tamir, "Leaky-wave antennas," in *Antenna Theory*, R. E. Colin and F. J. Zucker, Eds. New York: McGraw-Hill, 1969, ch. 20, pt. 2.
[5] A. A. Oliner, "Leaky-wave antennas," in *Antenna Engineering Handbook*, R. C. Johnson, Ed. New York: McGraw-Hill, 1993, ch. 10.
[6] N. G. Alexopoulos and D. R. Jackson, "Fundamental superstrate effects on printed circuit antennas," *IEEE Trans. Antennas Propag.*, vol. 32, pp. 807–816, Aug. 1984.
[7] D. R. Jackson and N. G. Alexopoulos, "Gain enhancement method for printed circuit antennas," *IEEE Trans. Antennas Propag.*, vol. 33, pp. 976–987, Sep. 1985.

[8] H. Y. Yang and N. G. Alexopoulos, "Gain enhancement method for printed circuit antennas through multiple superstrates," *IEEE Trans. Antennas Propag.*, vol. 35, no. 7, pp. 860–863, Jul. 1987.
[9] D. R. Jackson and A. A. Oliner, "A leaky-wave analysis of the high-gain printed antenna configuration," *IEEE Trans. Antennas Propag.*, vol. 36, no. 7, pp. 905–910, Jul. 1988.
[10] A. Ip and D. R. Jackson, "Radiation from cylindrical leaky waves," *IEEE Trans. Antennas Propag.*, vol. 38, pp. 482–488, Apr. 1990.
[11] D. R. Jackson, A. A. Oliner, and A. Ip, "Leaky-wave propagation and radiation for a narrow-beam multiple-layer dielectric structure," *IEEE Trans. Antennas Propag.*, vol. 41, no. 3, pp. 344–348, Mar. 1993.
[12] H. Ostner, J. Detlefsen, and D. R. Jackson, "Radiation from one dimensional dielectric leaky-wave antennas," *IEEE Trans. Antennas Propag.*, vol. 43, pp. 331–339, Apr. 1995.
[13] G. V. Trentini, "Partially reflecting sheet arrays," *IRE Trans. Antennas Propag.*, vol. AP-4, pp. 666–671, 1956.
[14] A. P. Feresidis and J. C. Vardaxoglou, "High gain planar antenna using optimised partially reflective surfaces," *Proc. Inst. Elect. Eng. Microw. Antennas Propag.*, vol. 148, no. 6, pp. 345–350, Dec. 2001.
[15] A. P. Feresidis, G. Goussetis, S. Wang, and J. C. Vardaxoglou, "Artificial magnetic conductor surfaces and their application to low profile high-gain planar antennas," *IEEE Trans. Antennas Propag.*, vol. 53, no. 1, pp. 209–215, Jan. 2005.
[16] T. Zhao, D. R. Jackson, J. T. Williams, and A. A. Oliner, "Simple CAD model for a dielectric leaky-wave antenna," *IEEE Antennas Wireless Propag. Lett.*, vol. 3, pp. 243–245, 2004.
[17] ——, "General formulas for 2-D leaky-wave antennas," *IEEE Trans. Antennas Propag.*, 2005, submitted for publication.
[18] G. Lovat, P. Burghignoli, and D. R. Jackson, "Fundamental properties and optimization of broadside radiation from uniform leaky-wave antennas," in *Proc. URSI General Assembly*, New Delhi, Oct. 2005.
[19] M. Thévenot, C. Cheype, A. Reineix, and B. Jecko, "Directive photonic bandgap antennas," *IEEE Trans. Microwave Theory Tech.*, vol. 47, pp. 2115–2122, Nov. 1999.
[20] C. Cheype, C. Serier, M. Thevenot, T. Monediere, A. Reinex, and B. Jecko, "An electromagnetic bandgap resonator antenna," *IEEE Trans. Antennas Propag.*, vol. 50, no. 9, pp. 1285–1290, Sep. 2002.
[21] Y. J. Lee, J. Yeo, R. Mittra, and W. S. Park, "Application of electromagnetic bandgap (EBG) superstrates with controllable defects for a class of patch antennas as spatial angular filters," *IEEE Trans. Antennas Propag.*, vol. 53, no. 1, pp. 224–235, Jan. 2005.
[22] A. R. Weily, L. Horvath, K. P. Esselle, B. C. Sanders, and T. S. Bird, "A planar resonator antenna based on a woodpile EBG material," *IEEE Trans. on Antennas Propag.*, vol. 53, no. 1, pp. 216–223, Jan. 2005.
[23] H.-Y. D. Yang, N. G. Alexopoulos, and E. Yablonovitch, "Photonic band-gap materials for high-gain printed circuit antennas," *IEEE Trans. Antennas Propag.*, vol. 45, pp. 185–187, Jan. 1997.
[24] B. Temelkuaran, M. Bayindir, E. Ozbay, R. Biswas, M. M. Sigalas, G. Tuttle, and K. M. Ho, "Photonic crystal-based resonant antenna with a very high directivity," *J. Appl. Phys.*, vol. 87, pp. 603–605, 2000.
[25] B. Gralak, S. Enoch, and G. Tayeb, "Anomalous refractive properties of photonic crystals," *J. Opt. Soc. Am. A*, vol. 17, pp. 1012–1020, 2000.
[26] A. Fehrembach, S. Enoch, and A. Sentenac, "Highly directive light sources using two-dimensional photonic crystal slabs," *Appl. Phys. Lett.*, vol. 79, pp. 4280–4282, Dec. 2001.
[27] G. Poilasne, P. Pouliguen, J. Lenormand, K. Mahdjoubi, C. Terret, and P. Gelin, "Theoretical study of interactions between antennas and metallic photonic bandgap materials," *Microwave Opt. Technol. Lett.*, vol. 15, pp. 384–389, 1997.
[28] G. Poilasne, P. Pouliguen, K. Mahdjoubi, C. Terret, P. Gelin, and L. Desclos, "Experimental radiation pattern of dipole inside metallic photonic bandgap material," *Microwave Opt. Technol. Lett*, vol. 22, pp. 10–15, 1999.
[29] K. C. Gupta, "Narrow beam antenna using an artificial dielectric medium with permittivity less than unity," *Electron. Lett.*, vol. 7, no. 1, p. 16, Jan. 1971.
[30] S. Enoch, G. Tayeb, P. Sabouroux, N. Guérin, and P. Vincent, "A metamaterial for directive emission," *Phys. Rev. Lett.*, vol. 89, pp. 213902-1–213902-4, Nov. 2002.
[31] P. Baccarelli, P. Burghignoli, F. Frezza, A. Galli, P. Lampariello, G. Lovat, and S. Paulotto, "Effects of leaky-wave propagation in metamaterial grounded slabs excited by a dipole source," *IEEE Trans. Microw. Theory Tech.*, vol. 53, pp. 32–44, Jan. 2005.
[32] G. Lovat, P. Burghignoli, F. Capolino, D. R. Jackson, and D. R. Wilton, "Analysis of directive radiation from a line source in a metamaterial slab with low permittivity," *IEEE Trans. Antennas Propag.*, vol. 54, no. 3, Mar. 2006.
[33] L. B. Felsen and N. Marcuvitz, *Radiation and Scattering of Waves*. Englewood Cliffs, NJ: Prentice Hall, 1973.
[34] G. Lovat, P. Burghignoli, and D. R. Jackson, "Fundamental properties and optimization of broadside radiation from uniform leaky-wave antennas," *IEEE Trans. Antennas Propag.*, 2005, submitted for publication.

Renato Gardelli was born in Messina, Italy, in 1976. He received the Laurea degree in electronic engineering from the University of Messina, Italy, in 2002, where he is currently working toward the Ph.D. degree in electromagnetic engineering.

His research interests are in the area of microstrip antennas design, electromagnetic band-gap structures and frequency selective surfaces.

Matteo Albani (M'98) was born in Florence, Italy, in 1970. He received the Laurea degree (*cum laude*) in electronic engineering and the Ph.D. degree in telecommunications and electronic engineering from the University of Florence, Florence, Italy, in 1994 and 1998, respectively.

From 1999 to 2001, he was an Associate Researcher with the Department of Information Engineering (DII), University of Siena, Italy. In 2001, he joined the Department of Matter Physics and Advanced Physical Technologies, University of Messina, Italy, as an Assistant Professor. Since 2005, he has again been associated to the DII. His research interests encompass high-frequency methods for electromagnetic scattering and propagation, numerical methods for large array antennas, antenna analysis and design.

Dr. Albani was awarded with the "Giorgio Barzilai" prize for the Best Young Scientist paper during the Italian National Conference on Electromagnetics in 2002 (XIV RiNEm) and with a Young Scientist Award for participating in the URSI International Symposium on Electromagnetics in 2004.

Filippo Capolino (S'94–M'97–SM'04) was born in Florence, Italy, in 1967. He received the Laurea degree (*cum laude*) in electronic engineering and the Ph.D. degree from the University of Florence, Florence, Italy, in 1993 and 1997, respectively.

From 1994 to 2000, he was a Lecturer in antennas, from 2000 to 2002, he was a Research Associate, and since 2002, has been an Assistant Professor at the University of Siena, Italy. From 1997 to 1998, he was a Fulbright Research Visitor with the Department of Aerospace and Mechanical Engineering, Boston University, Boston, MA, where he continued his research with a Grant from the Italian National Council for Research (CNR), from 1998 to 1999. From 2000 to 2001, he was a Research Assistant Visiting Professor with the Department of Electrical and Computer Engineering, University of Houston, Houston, TX, where he is now an Adjunct Assistant Professor. From November to December 2003, he was an Invited Assistant Professor at the Institut Fresnel, Marseille, France. His primary research interests are in high-frequency, short-pulse radiation, array antennas, periodic structures, and metamaterials. He is the coordinator of the Siena Unit for the Network of Excellence "Metamorphose" on Metamaterials of the EU FP6.

Dr. Capolino was awarded with an MMET'94 Student Paper Competition Award in 1994, the Raj Mittra Travel Grant for Young Scientists in 1996, the "Barzilai" prize for the best paper at the National Italian Congress of Electromagnetism (XI RiNEm) in 1996, and a Young Scientist Award for participating at the URSI International Symposium on Electromagnetics Theory in 1998. He received the R. W. P. King Prize Paper Award from the IEEE Antennas and Propagation Society for the Best Paper of the Year 2000, by an author under the age of 36. He is an Associate Editor for the IEEE TRANSACTIONS OF ANTENNAS AND PROPAGATION.